Polyhedron 81 (2014) 475–484

Contents lists available at ScienceDirect

Polyhedron

journal homepage: www.elsevier.com/locate/poly

Microwave-assisted silylation of graphite oxide and iron(III) porphyrin intercalation

Monika E. Lipińska [a], João P. Novais [a], Susana L.H. Rebelo [a,*], Belén Bachiller-Baeza [c], Inmaculada Rodríguez-Ramos [c], Antonio Guerrero-Ruiz [b], Cristina Freire [a,*]

[a] REQUIMTE, Departamento de Química e Bioquímica, Faculdade de Ciências, Universidade do Porto, Rua Campo Alegre s/n, 4169-007 Porto, Portugal
[b] Dpto. de Química Inorgánica y Química Técnica, Facultad de Ciencias, UNED, Senda del Rey 9, 28040 Madrid, Spain
[c] Instituto de Catálisis y Petroleoquímica, CSIC, C/Marie Curie 2, Cantoblanco, 28049 Madrid, Spain

ARTICLE INFO

Article history:
Received 28 March 2014
Accepted 2 July 2014
Available online 10 July 2014

Keywords:
Graphite oxide
Iron(III) porphyrin
Microwave-assisted synthesis
Silylation
Catalysis

ABSTRACT

The hybrid material graphite oxide (GO) intercalated with an iron(III) porphyrin was obtained upon a silylation reaction of GO with 3-bromotrimethoxypropylsilane (BrTMS) followed by metalloporphyrin immobilization. Diverse reaction conditions and microwave *versus* conventional heating were tested. The materials were characterized using X-ray diffraction (XRD), X-ray photoelectron spectroscopy (XPS), Fourier-transform infrared spectroscopy (FTIR), thermogravimetry (TGA) and temperature programmed desorption (TPD). Microwave-assisted synthesis allowed functionalization reactions of 1 h instead of 24 h (conventional heating) with equivalent or improved yields on both silylation and metalloporphyrin immobilization reactions. The immobilizations performed in anhydrous solvent and absence of other exfoliation agents led to an increase on the GO interlayer distance of 0.14 nm, in a total space of 7 Å that match the metalloporphyrin thickness.

1. Introduction

Graphite oxide (GO) is a layered carbon material with high hydrophilic character, owing to the presence of a significant amount of oxygen groups, mainly epoxy and hydroxy groups in the basal layer surfaces or carboxylic groups in the edges of the graphene sheets [1]. These functional groups assure good dispersibility, easy processability and compatibility with other materials, being particularly prone to obtain further functionalizations [2,3]. Moreover, the swelling and exfoliation capabilities ensure the formation of solid matrices and host materials, allowing the intercalation of different molecules and the construction of supramolecular systems [4]. Together with the good mechanical properties and the large surface area of GO, these inherent characteristics made of this material one of the most promising carbon materials for different applications [5], like photochemical reactions [6], drug delivery [7] and catalysis [8–11].

Derived materials can be originated from chemical and temperature treatments of GO as reduced GO [12], GO framework materials [13] or pillared GO [14]. Moreover, the functionalizations enable the fine tuning of surface properties, which is important to obtain selective adsorption and dispersibility in different solvents [15]. In this context, the grafting of silicon-containing molecules on GO, such as polymers [16] or organosilanes [17,18], provides straightforward covalent functionalization strategies. Most of the up to date studies have been focused on the anchoring of chloro- and alkoxysilanes carrying an extended aliphatic chain or with a second functionality, in order to increase the interlayer distances or allow the anchoring of other moieties. These studies revealed that the organosilanes mainly react with the hydroxyl groups on the GO surface to establish Si–O-GO bonds [19,20]. The presence of exfoliating or stabilizing agents was also considered [21,22], but its excess showed to prevent the attack of organosilane on the GO surface, thus reducing the extension of the reaction [21].

When aminoalkylethoxysilanes were used, the organosilane moieties or coupling dimmers can bind to two different superimposed GO sheets, through nucleophilic attack on the silane ethoxy groups by OH-GO functionalities and by amidation reaction on the HOOC-GO groups or nucleophilic attack on epoxy-GO groups [23]. This can led to structures with stable interlayer distance, assuring a good dispersion, avoiding aggregation and enabling the formation of the matrices for molecules intercalation.

* Corresponding authors. Tel.: +351 220402590; fax: +351 220402695.
E-mail addresses: susana.rebelo@fc.up.pt (S.L.H. Rebelo), acfreire@fc.up.pt (C. Freire).

http://dx.doi.org/10.1016/j.poly.2014.07.003
0277-5387/

Metalloporphyrins have been extensively investigated in different fields, such as in artificial photosynthesis, in medicine and catalysis [24]. For all these applications, the development of suitable methodologies for their immobilization on appropriate supports is presently a goal of huge relevance. Hybrids of porphyrinic chromophores and GO have been prepared as donor–acceptor structures for solar light energy conversion, non-linear optical absorption [25–27] and biosensing [28]. Thus, the application of GO as a versatile, easily available and inexpensive support for metalloporphyrin catalysts or as carrier for metalloporphyrins with biological activity or sensing capabilities is very promising [29–33], although, in practice, these have been quite unexplored fields.

Herein, an iron(III) porphyrin carrying tetrafluorodimethylamino groups was immobilized onto GO (Fig. 1). Initially, the silylation of GO with 3-bromopropyltrimethoxysilane (BrTMS) was developed followed by metalloporphyrin intercalation; both reactions were optimized screening reaction conditions and using microwave *versus* conventional heating [34,35]. The epoxidation of *cis*-cyclooctene was used as a proof of concept for the iron(III) porphyrin immobilization on its catalytic-active form.

2. Experimental

2.1. Materials

All reagents and solvents were used as received without further purification. In the synthesis reactions and catalytic studies were used: natural graphite powder (99.999% stated purity, 200 mesh, Alfar Aesar), fuming nitric acid (>90%, Panreac), potassium chlorate (ACS Reagent + 99%, Sigma–Aldrich), pentafluorobenzaldehyde (⩾98%, Alfa Aesar), pyrrole (98%, Sigma–Aldrich), diethyl ether (⩾98%, Merck), dichloromethane (98%, Fischer), methanol (>99.8%, Chem-Lab NV), iron(II) chloride ($FeCl_2{\cdot}4H_2O$, Merck), chloroform (98%, Fischer), 3-bromopropyltrimethoxysilane (BrTMS, ABCR), anhydrous toluene (⩾99.8%, Sigma–Aldrich), *cis*-cyclooctene (95%, Sigma–Aldrich), decane (⩾99%, Sigma–Aldrich), hydrogen peroxide ($H_2O_{2(aq)}$ 30% (w/w), Sigma–Aldrich), *N*,*N*-dimethylformamide (DMF, 98%, Fischer), *N*-methyl-2-pyrrolidone (NMP, ⩾99%, Sigma–Aldrich), ethanol absolute (98%, Fischer), *o*-dichlorobenzene anhydrous (>99%, Aldrich). In all filtration procedures were used 0.2 μm polyamide membrane filters (NL16 Whatman).

2.2. Physicochemical characterization

Powder X-ray diffractograms (XRD) were recorded on a Polycristal XPert Pro PANalytical apparatus using Ni-filtered Cu Kα radiation (λ = 0.15406 nm) and a graphite monochromator. For each sample, Bragg's angles between 4° and 90° were scanned at a rate of 0.04°/s.

X-ray photoelectron spectroscopy (XPS) was performed on ESCAPROBE P spectrometer from OMICRON equipped with EA-125 hemispherical multichannel Electronics analyzer. The excitation source was the Mg Kα line ($h\nu$ = 1253.6 eV, 300 W). The error in determination of electron binding energies and line widths did not exceed 0.2 eV. The raw XPS spectra were deconvoluted by curve fitting of the peak components using the software XPSPEAK 4.1 with no preliminary smoothing. Symmetric Gaussian–Lorentzian product functions were used to approximate the line shapes of the fitting components after a Shirley-type background subtraction. Atomic ratios were calculated from experimental intensity ratios and normalized by atomic sensitivity factors.

Fourier transform infrared spectra (FTIR) of the materials were collected in a Jasco FT/IR-460 Plus spectrophotometer in the 400–4000 cm^{-1} range with a resolution of 4 cm^{-1} and 32 scans. The spectra were obtained in KBr pellets containing 0.2% weight of GO materials.

Thermogravimetric analysis (TGA) was performed on a CI Electronics microbalance (MK2-MC5). All samples (typically 10 mg) were heated under helium flow to 850 °C at a rate 5 °C/min.

Temperature programmed desorption – mass spectroscopy (TPD–MS) experiments were carried out under vacuum in a conventional volumetric apparatus connected to a SRS RGA-200 mass spectrometer. The sample was evacuated for 30 min at room temperature and then ramped to 700 °C at a rate 5 °C/min.

GC-FID chromatograms were obtained with a Varian CP-3380 gas chromatograph equipped with a FID detector, using hydrogen as carrier gas and a fused silica Varian Chrompack capillary column CP-Sil 8 CB Low Bleed/MS (30 m × 0.25 mm id; 0.25 μm film thickness). The epoxidation reactions were followed with temperature program: 70 °C (1 min), 20 °C min^{-1}, 200 °C (8 min); injector temperature: 200 °C; detector temperature: 250 °C.

2.3. Microwave synthesis

Microwave synthesis was carried out using CEM Discover LabMate reactor with pressure and temperature control system in 10 mL reaction vessel. The reaction mixture was constantly irradiated in closed system using 150 W maximum power at the desired temperature.

2.4. Preparation of the materials

2.4.1. Preparation of graphite oxide (GO)

Graphite oxide was synthesized from natural graphite powder using a modified Brodie's method [36]. Typically, 10 g of graphite was added to 200 mL of fuming HNO_3, which was previously cooled to 0 °C in an iced bath. Then 80 g of potassium chlorate was slowly added. The reaction mixture was kept under stirring for 21 h, then filtered. Obtained material was extensively washed with deionized water until neutral pH and dried under vacuum at 60 °C overnight.

2.4.2. Synthesis of iron(III) porphyrin (FeP)

The base porphyrin H_2TPFPP and its iron(III) complex were synthesized through previously reported methodologies [37]. However, in the pyrrole and pentafluorobenzaldehyde condensation reaction, nitrobenzene as hazardous solvent was eliminated and

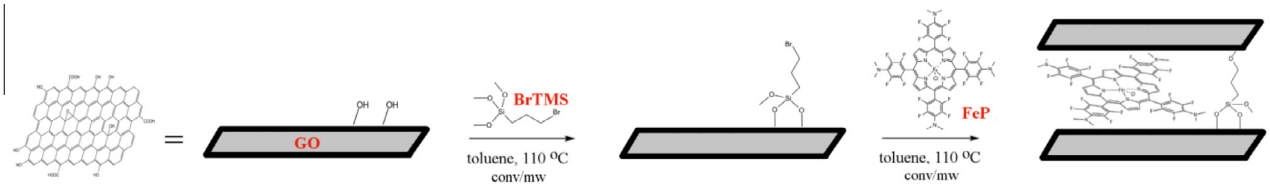

Fig. 1. Schematic representation of the GO silylation with bromosilane followed by iron(III) porphyrin immobilization. Both reactions were carried out in toluene at 110 °C using conventional and microwave heating.

the reaction was carried out in glacial acetic acid. The complexation of the free porphyrin with iron(II) chloride in refluxing DMF [38] led to the *meso*-tetrakis-(4-*N*,*N*-dimethylamine-2,3,5,6-tetrafluoro)porphyrinate iron(III) chloride denoted as **FeP**.

2.4.3. Silylation of graphite oxide (sGO)

In order to obtain optimized conditions, different heating modes (conventional or microwave), solvents (toluene, DMF, NMP), reaction times and temperatures were tested as described in Table 1.

Method 1 (conventional heating – *ch*): In a typical reaction, 800 mg of GO were sonicated for 30 min in 200 mL of the chosen solvent and then 0.15 mL of BrTMS were added. The reaction mixture was refluxed under argon atmosphere during 24 h. Then, the solid was filtered, washed, dispersed again in a new portion of 200 mL of the reaction solvent, sonicated for 10 min and refluxed during 1 h. After the filtration, the material ***sGOch*** was extensively washed with the reaction solvent and diethyl ether and finally dried under vacuum at 120 °C overnight.

Method 2 (microwave-assisted synthesis – *mw*): In a typical reaction, 200 mg of GO were sonicated for 30 min in 8 mL of the chosen solvent and then 0.04 mL of BrTMS were added to the reaction vessel. The vessel was introduced in the microwave apparatus and reaction was heated and irradiated, following the conditions presented in Table 1, at a pressure of 200 psi. Then, the solid was filtered, washed, transferred to a round bottom flask, again dispersed in 200 mL of the same solvent, sonicated during 10 min and refluxed during 1 h. After the filtration, the material ***sGOmw*** was extensively washed with the reaction solvent and diethyl ether and finally dried under vacuum at 120 °C overnight.

2.4.4. Preparation of FeP-sGO materials

In order to obtain optimized conditions, different heating modes (conventional or microwave), solvents (toluene, NMP), reaction times and temperatures were tested as described in Table 5.

Method 1 (conventional heating – *ch*): In a typical reaction, 80 mg of FeP were added to 400 mg of sGO*ch1* and sonicated during 30 min in 120 mL of the chosen solvent. The reaction mixture was refluxed under argon atmosphere for 24 h. Then, the solid was filtered, rinsed and dispersed in a new portion of 120 mL of the reaction solvent, sonicated during 10 min and refluxed during 1 h. After the filtration, the material **FeP-sGO*ch*** was extensively washed with the reaction solvent, ethanol and diethyl ether and finally dried under vacuum at 120 °C overnight.

Method 2 (microwave-assisted synthesis – *mw*): In a typical reaction, 40 mg of FeP and 200 mg of *s*GO*mw* were put in the reaction vessel and dispersed in 8 mL of the chosen solvent by sonication during 30 min. The vessel was introduced in the microwave apparatus and the reaction mixture was heated and irradiated, at the pressure of 200 psi. After that time the solid was filtered, washed, transferred to a round bottom flask, dispersed again in 60 mL of clean reaction solvent and followed by sonication during 10 min and reflux during 1 h. After the filtration by the previous procedure, the material **FeP-*sGOmw*** was extensively washed with the reaction solvent, ethanol and diethyl ether and finally dried under vacuum at 120 °C overnight.

Table 1
Experimental conditions used for GO silylation in the different synthesis.

Entry	Material	Heating	Solvent	T (°C)	t (h)	Other
1	*sGOch1*	conventional	toluene	110	24	
2	*sGOch2*	conventional	toluene	60	5	
3	*sGOmw1*	microwave	toluene	110	1	
4	*sGOmw2*	microwave	toluene	110	2	
5	*sGOmw3*	microwave	toluene	110	1	Open vessel
6	*sGOmw4*	microwave	DMF	140	1	
7	*sGOmw5*	microwave	NMP	200	1	

2.4.5. Direct reaction of FeP and GO

About 250 mg of GO were dispersed in 200 mL of NaOH 0.015 M and stirred for 1 h at 100 °C. The obtained material was washed with water until pH 8, filtered and dried in the oven. To 200 mg of this material and 40 mg of FeP were added 8 mL of *o*-dichlorobenzene and the mixture was sonicated for 30 min. The vessel was introduced in the microwave apparatus and the reaction mixture was heated at 180 °C and irradiated at the pressure of 200 psi. After that time the solid was filtered, washed, dispersed again in 60 mL of the solvent, sonicated for 10 min and refluxed during 1 h. After the filtration by the previous procedure, the material **FeP-GO*mw*** was extensively washed with the clean *o*-dichlorobenzene, ethanol and diethyl ether and finally dried under vacuum at 120 °C overnight.

2.5. Catalytic studies

2.5.1. Epoxidation of cis-cyclooctene

Typically the reaction mixture was prepared by dissolving 0.5 mmol of *cis*-cyclooctene and 0.2 mmol of decane as internal standard, in 1.5 mL of ethanol. To this mixture 25 mg of the material to be tested as catalyst were added followed by sonication during 15 min. Then, the mixture was kept under magnetic stirring, protected from light and at controlled temperature between 20 and 23 °C. The oxidant [H_2O_2 30% w/w (aq.)], diluted 1:10 in ethanol, was progressively added in aliquots of 0.5 or 0.25 mmol, at 1 h intervals. After 55 min of each oxidant addition the reaction was sonicated during 5 min in order to disperse the material, an aliquot of this mixture was removed for GC analysis and a novel oxidant aliquot was added. To perform GC analysis, 0.1 mL of reaction mixture was sampled, centrifuged (15 min, 6000 rpm) to separate the solid and the supernatant was directly injected on the GC.

2.5.2. Catalytic parameters

Conversion (C%) was determined both by calculation of reacted substrate using the internal standard method ($A_{i.s.}$ = area of internal standard) and based on the chromatographic peak areas of substrate ($A_{sub.}$) and products ($A_{prod.}$) for each chromatogram. The conversion values obtained with both procedures always agreed within 5%.

$$C\% = \frac{\left(\frac{A_{sub.}}{A_{i.s.}}\right)_{t=0} - \left(\frac{A_{sub.}}{A_{i.s.}}\right)_{t=xh}}{\left(\frac{A_{sub.}}{A_{i.s.}}\right)_{t=0}} \times 100$$

$$C\% = \frac{A_{prod.}}{A_{sub.} + A_{prod.}} \times 100$$

The product selectivity was also calculated based on the chromatographic peak areas and calculated as follows:

$$S\% = [A_{epoxide}] \times 100/[A_{prod.}]$$

The turnover number (TON) was calculated through the ratio between the number of mols of the converted substrate ($n_{conv.sub.}$) and the mol of the metalloporphyrin in the catalyst (n_{FeP}) and the turn over frequency (TOF) was determined by the calculation of TON after the 1 h of the reaction ($TON_{t=1h}$). The n_{FeP} corresponds to the iron loading obtained by XPS, in mmol/g (material).

$$TON = \frac{n_{conv.sub.}}{n_{FeP}}$$

$$TOF = TON_{t=1h}$$

3. Results and discussion

3.1. Organosilylation of graphene oxide

The preparation of iron(III) porphyrin-GO hybrid was preceded by the development of a practical procedure for GO silylation with 3-bromopropyltrimethoxysilane (BrTMS). Previous studies revealed that the effectiveness of GO silylation depends on the temperature and reaction time, as well as, on the presence of silane polymerization inducers, such as water or exfoliating agents [16,21]. The silylation of GO with BrTMS was developed by testing different conditions as summarized in Table 1.

The reaction was carried out using conventional heating at 110 °C, during 24 h in anhydrous toluene in order to avoid polymerization and loss of bromide from the alkyl bromide functional groups; from this synthesis resulted material *s*GO*ch1* (entry 1, Table 1). Longer reaction times have shown to not improve silylation efficiency [21]. Due to the labiality of the alkylbromine moiety, milder silylation conditions were also tested. In accordance, the silylation was performed in the same solvent but at 60 °C during 5 h (entry 2) to afford material *s*GO*ch2* [16].

The microwave irradiation was tested in reflux of anhydrous toluene, during 1 h (entry 3) or 2 h (entry 4), leading to materials *s*GO*mw1* and *s*GO*mw2*, respectively. Using the same conditions as in entry 3, the reaction was also performed in "open vessel" condition, due to the possibility of using bigger reaction volumes and increasing the reaction scale (*s*GO*mw3*, entry 5). Higher reaction temperatures were also tested using higher boiling point solvents, such as DMF (*s*GO*mw4*, entry 6) and NMP (*s*GO*mw5*, entry 7), which also could led to an increased exfoliation/dispersion of GO [39].

3.2. Physicochemical characterization of silylated graphite oxide

The XRD diffractograms of GO and silylated GO materials – sGO*ch1*, sGO*ch2* and sGO*mw1* – are collected in Fig. 2. The diffraction peak of GO is observed at $2\theta = 15.8°$ that corresponds to lattice parameters (001) and a d-spacing of 0.564 nm (Table 2). This indicates a graphite oxidation in a median extension relatively to other functionalization protocols described in the literature [40], aiming to provide enough functional groups to obtain further derivatizations, without a strong disruption of the graphene layers planar structure. The diffraction peak characteristic for graphite at $2\theta = 26°$ is absent in GO material, and this indicates the homogeneous functionalization/oxidation of graphite that is being observed in one single phase.

Table 2
The X-ray diffraction angels and corresponding interlayer distances.

Material	2θ (°)	d (nm)[a]
GO	15.8	0.564
sGOch1	13.4	0.660
sGOch2	15.4; 15.7	0.575; 0.564
sGOmw1	13.0	0.685
FeP-*sGOch1*	12.6	0.702

[a] d-Spacing corresponding to the main (1 0 0) XRD reflection: $d_{100} = \lambda/(2\sin\theta)$.

The diffraction peak of silylated material *sGOch1* (entry 1, Table 1), is observed at $2\theta = 13.4°$ and indicates an increase in the interlayer distance to 0.660 nm caused by the introduction of organosilane [14]. In the material *sGOch2* synthesized at lower temperatures and lower reaction time (60 °C during 5 h, entry 2), two diffraction peaks at $2\theta = 15.4°$ and 15.7° are observed, what evidences the co-existence of poorly silylated and non silylated regions on GO [21] and confirms the inefficiency of the experimental conditions used.

On the other hand, using microwave assisted synthesis, upon 1 h of the reaction time (Table 1, entry 3) *sGOmw1* exhibits the diffraction peak at $2\theta = 13.0°$, which corresponds to an interlayer distance of 0.685 nm, slightly larger compared with the material *sGOch1* prepared by the conventional heating. The intensity of the diffraction peaks of the *s*GO materials decreased relatively to GO, also corroborating the introduction of the silane moieties in the interlayers of the material.

Table 3 summarizes the XPS surface atomic percentages for the synthesized materials. The original GO presents 75.2% of carbon and 24.8% of oxygen atoms. After reaction with BrTMS using conventional and microwave-assisted heating to afford materials *sGOch1*, *sGOmw1* and *sGOmw2*, the carbon percentage was practically maintained, although, the oxygen percentage decreased of *ca.* 1.2% at the expense of the appearance of silicon and bromine elements. The material *sGOch1* shows 1.1% of Si (830 μmol·g^{-1}) and 0.2% of Br (150 μmol·g^{-1}). The low atomic ratio Br/S = 0.2, relatively to the expected Br/S = 1, is the consequence of the labiality of the alkylbromine moiety and its probable reaction with nucleophilic groups. It can be hypothesized that some of the organosilane units are bonded to both superior and inferior sheets (resulting from reaction of the methoxy groups in one side and by reaction of the alkylbromine moieties with the hydroxyl groups in the other side); this can maintain a stable interlayer distance and form a more appropriate host material.

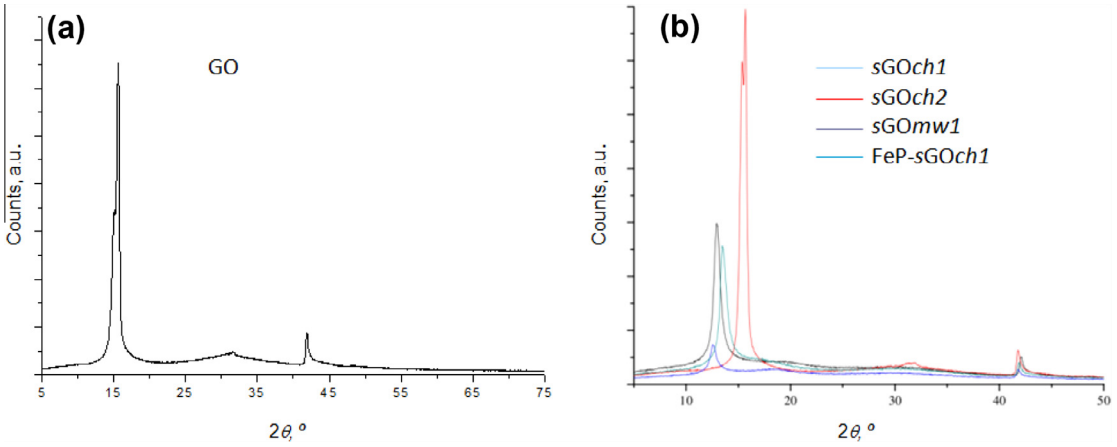

Fig. 2. XRD diffractograms for (a) original GO and (b) functionalized materials.

Table 3
Surface atomic percentages of materials obtained by XPS.[a]

	At%							
Sample	C1s	O1s	Si2p$_{3/2}$	Br3d$_{5/2}$	N1s	F1s	Fe2p$_{3/2}$	Cl2p$_{3/2}$
GO	75.2	24.8						
sGOch1	75.1	23.6	1.1	0.2				
sGOmw1	75.1	23.8	0.9	0.2				
sGOmw2	75.1	23.4	1.3	0.2				
sGOmw3	75.2	24.7	0.1	0.02				
FeP-*sGOch1*	74.4	20.5	0.8	–	2.0	2.0	0.1	0.2
FeP-*sGOmw1*	72.9	21.7	0.4	–	1.8	2.7	0.2	0.3
FeP-*sGOmw2*	73.3	21.1	0.5	–	1.8	2.8	0.2	0.3

[a] Determined by the areas of the respective bands in the high-resolution XPS spectra.

Materials *sGOmw1* and *sGOmw2* show Si% in the range 0.9 – 1.3% although the Br% = 0.2 is identical for the three materials. Thus, the results evidence identical functionalization degree for the three materials and attest the advantage of the microwave-assisted synthesis relatively to conventional heating, which allows lower consumption of time and energy. Furthermore, these results allow concluding that there is no advantage in extending the reaction time for more than 1 h in the microwave protocol.

The corresponding high resolution spectra of the relevant elements of GO and *sGOmw1* materials are collected in Fig. 3. Very similar spectral patterns are observed for *sGOch1*; the corresponding spectra are presented in Fig. 1a, SI.

The XPS high resolution spectrum of GO in the C1s region was deconvoluted into four bands (Fig. 3a). The small peak at the lowest binding energy (B.E.), at 283.7 eV is ascribed to carbon in the graphitic structure and aromatic rings (sp^2); the peak at 285.1 eV to carbon–carbon single bond in the carbon structure (sp^3). The other two peaks are associated with the presence of the oxygen-containing groups: the peak at 286.9 eV with the hydroxyl and epoxy/ether groups (C–O) and the smaller peak at 288.6 eV with the carbonyl/carboxyl groups (C=O). In the O1s region spectrum two peaks are present: a small peak at 529.3 eV is assigned to O=C bond and a much more intense at 531.2 eV to O–C bond, suggesting that hydroxyl or epoxide groups are more abundant than the carboxylic acid groups [41].

The C1s spectrum of *sGOmw1* (Fig. 3b) shows a small increase in the intensity of the band at 283.9 eV, which is related with the contribution of C–Si band due to the grafted organosilane [16]. In the O1s region of this material there are some shifts in the peak positions and the band at 529.4 eV is relatively more intense than the corresponding band in GO O1s spectrum, what is a result of the contribution of O–Si band from the grafted organosilane [19]. The Si2p spectrum shows a broad band at 103.1 eV, being a slightly higher B.E. than the typical values observed for Si–OH and Si–O–C bonds and was previously observed when these peaks are overlapped by peaks due to the presence of Si–O–Si bonds, the latter being a consequence of polymerization or intermolecular silane coupling [19]. Even if an anhydrous solvent was used, the highly polar and protonic GO surface can catalyze the hydrolysis of the methoxy groups from the organosilane and consequently, these Si–OH groups can undergo nucleophilic attack on the silicon atom of one other silane molecule [40]. So, it can also be considered that some organosilane dimmers or polymers are present.

In the Br3d3 spectrum it can be observed a band at B.E. 76.8 eV ascribed to the presence of Br–C bond in the alkyl chain of alkylbromosilane [35].

The FTIR spectrum of GO is depicted in Fig. 4 and shows peaks related with the oxygen-containing groups present on its surface and with the carbon structure. The bands at 3460 cm^{-1} (ν O–H), 1740 cm^{-1} (ν C=O), 1620 cm^{-1} (δ O–H), 1390 cm^{-1} (δ C–OH), 1060 cm^{-1} (ν C–O) are endorsed to hydroxyl, carboxyl and epoxy groups. Some of these bands are overlapped by the vibrations from the carbon structure, at 1620 cm^{-1} (ν C=C) and at 1060 cm^{-1} (C–C skeletal tangential motions) [42]. The spectrum also confirms the presence of higher amounts of hydroxyl and epoxy groups than carboxylic functionalities.

After the silylation, the most notorious changes in the spectral features are related with the introduction of three bands, centered at 2920 cm^{-1} (ν C–H) together with the shoulder at near 1480 cm^{-1} (δ C–H) in accordance with the introduction of alkyl and alkoxy chains from grafted organosilane [42]. The series of the bands between 1200 and 1000 cm^{-1} are also assigned to asymmetric stretching vibrations of Si-O-R groups [19].

The TGA curve of GO in an inert atmosphere (Fig. 5) shows that GO is thermally stable up to *ca.* 250 °C, where occurs an intense mass decrease associated with the pyrolysis of the label oxygen groups and release of different gases (see below the TPD analyzes). After this temperature, GO shows a progressive, slow rate mass loss up to a total mass loss of 34% (Table 4).

The silylated materials show thermogravimetric profiles similar to original GO (Fig. 5 and Fig. 2, SI). For material *sGOch1* the strong mass loss occurred at a slightly lower temperature relatively to GO (Fig. 5) and from Table 4, it can be seen that the final total mass loss increased to 37% relatively to the 34% observed for original GO. Material *sGOch2* does not show higher mass loss relatively to GO, corroborating the very low functionalization indicated previously. Material *sGOmw2* showed the highest mass loss among the silylated materials, namely 44%, in the region 200–300 °C, and is observed at slightly lower temperature compared with GO. Other materials silylated with BrTMS also showed a decomposition step in the range 200–300 °C [35].

Temperature-programmed desorption (TPD) was performed monitoring the release of possible degradation fragments, namely *m/z* 44 (CO_2), 28 (CO); 18 (H_2O), 32 (O_2), 2 (H_2), 43 ($CH_3CH_2CH_2$), 42 ($CH_2CH_2CH_2$), 80 (HBr), 27 (CH_3CH_2), 94 (CH_3Br). In the analyzed temperature range the most significant fragments in GO were CO_2, CO, H_2O, and H_2, while in silylated materials were CO_2, CO, H_2O and the fragment with *m/z* 43 from the $CH_3CH_2CH_2$ moiety. The results in the temperature range of 150–450 °C are shown Fig. 3, SI, since in the temperature range of 450–750 °C no significant gas release was observed.

The oxygenated surface groups are thermally decomposed releasing CO and/or CO_2 and the decomposition temperature and the type of the gas released during the analysis give information about the nature of the groups [19]. Water molecules are present in the interlayer space and maintain the GO structure by hydrogen bridging. The detection of the fragment *m/z* 43 further confirmed the occurrence of the silylation reaction. The CO_2 release at lower temperature (near 300 °C) is associated with the decomposition of carboxylic acids groups, while the CO release near that temperature results from the decomposition of the epoxy or non-aromatic hydroxyl groups, since phenolic hydroxyl or quinone groups decompose releasing CO at higher temperatures, near 800 °C, and phenolic groups positioned in the deep basal planes are expected to decompose at even higher temperatures. In our case these last decompositions are above the monitoring range [19].

In Fig. 6 and in Fig. 3, SI, the TPD profiles of the materials show that CO_2 is the gas released in the highest amount, followed by water and carbon monoxide. This observation, although commonly observed in the TPD of GO materials [43,14], apparently contrast with the higher number of hydroxyl groups relatively to carboxylic groups observed by the previously discussed techniques, namely XPS and FTIR. This can be explained considering that only non-aromatic hydroxyl groups and epoxy moieties are being monitored in the studied temperature range and not the hydroxyl groups from phenolic moieties, which are expected at higher temperatures [44].

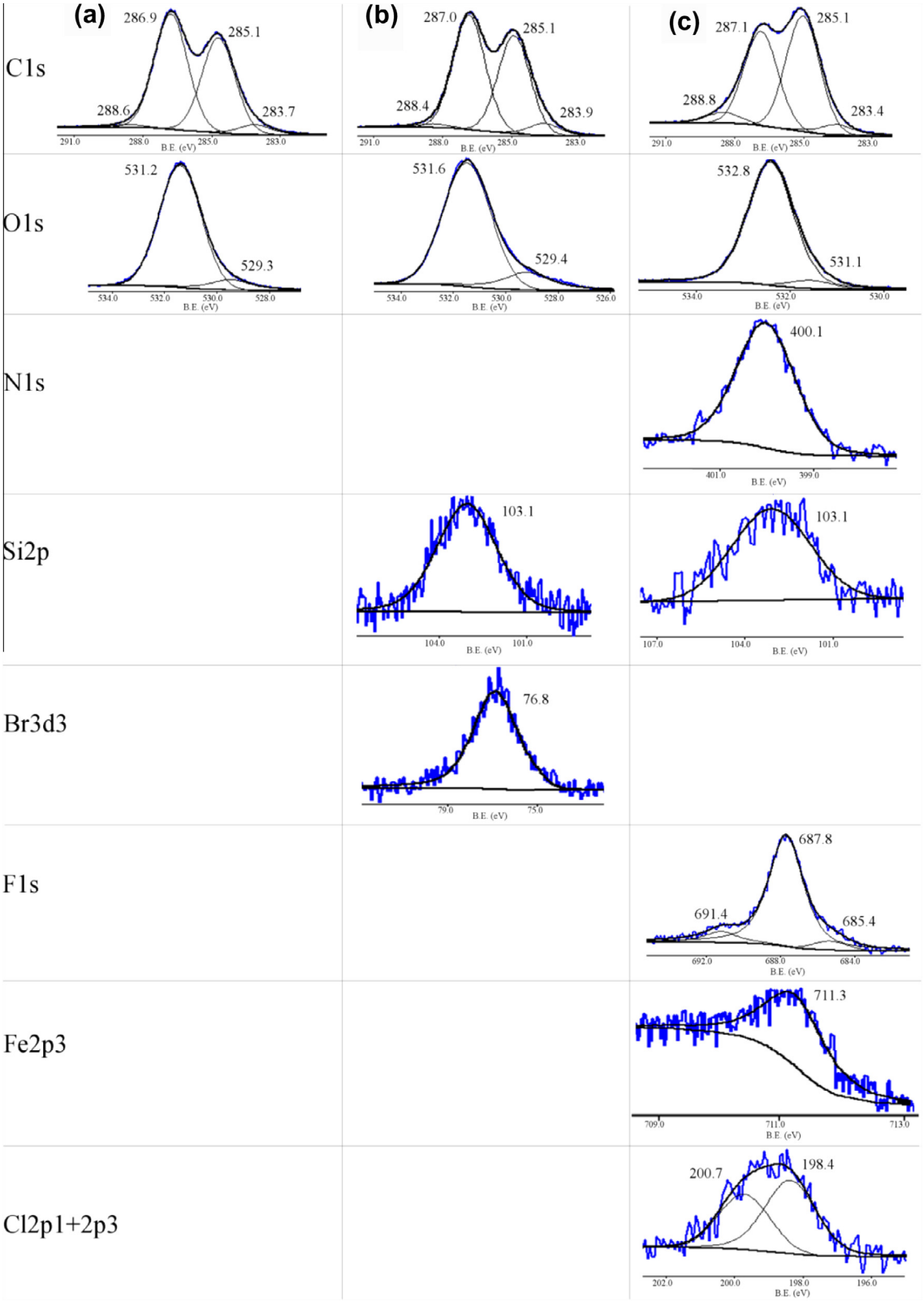

Fig. 3. XPS high resolution spectra of relevant elements present on materials: (a) GO; (b) *s*GO*mw1*; (c) FeP-*s*GO*mw1*.

It can also be observed that in material *s*GO*ch1* the amount of CO_2 is lower than for original GO and for material *s*GO*mw2* (Fig. 6a); this can be related with the longer reaction times used in the conventional heating protocol, with increased decomposition of the material, namely of carboxylic groups. On the other hand, CO is released in lower amount from material *s*GO*mw2* than from original GO (Fig. 6b); this can confirm the silylation reaction of the OH groups from GO. However, in material *s*GO*ch1* the CO peak approach the one of GO, which is probably due to increased hydrolysis of the organosilane methoxy groups to hydroxylated

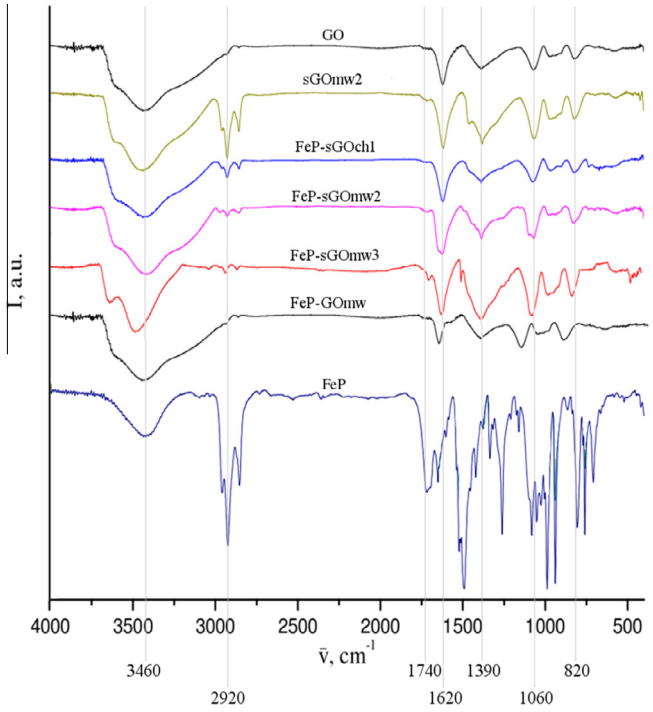

Fig. 4. Representative FTIR spectra of GO, *sGOmw2*, FeP-*sGOch1*, FeP-*sGOmw2*, FeP-*sGOmw3* and FeP-GO*mw* materials in comparison with FeP.

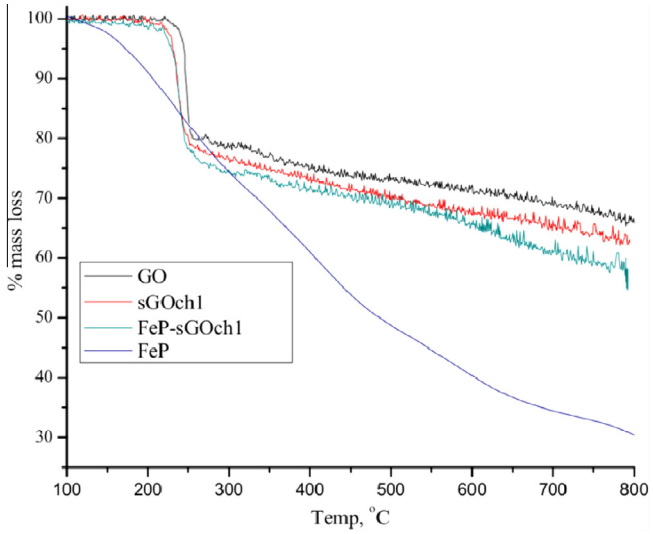

Fig. 5. Thermograms of GO, *sGOch1*, FeP-*sGOch1* and FeP materials in an inert atmosphere.

Table 4
Total mass losses (%) obtained by TG analysis.

Material	% Total mass loss
GO	34
sGOch1	37
sGOch2	31
sGOmw2	44
FeP-*sGOch1*	42
FeP-*sGOmw2*	43
FeP	79

derivatives, due to the longer reaction times with exposition to humidity and temperature. The higher amount of water released

Table 5
Experimental conditions for the immobilization of the Fe(III)porphyrin.

Entry	Material	Heating	Solvent	T (°C)	*t* (h)
1	FeP-*sGOch1*	conventional	toluene	110	24
2	FeP-*sGOmw1*	microwave	toluene	110	1
3	FeP-*sGOmw2*	microwave	toluene	110	2
4	FeP-*sGOmw3*	microwave	NMP	200	1
5	FeP-GO*mw*[a]	microwave	*o*-dichlorobenzene	180	1

[a] Reaction of metalloporphyrin directly on GO (non-silylated).

for this material confirms this hypothesis (Fig. 6c). The results give evidence for the better maintenance of materials integrity upon microwave functionalization relatively to the procedure under conventional heating. The temperatures of the CO_2, CO and H_2O decomposition peaks match the steps of mass loss observed on thermogravimetry analyzes.

3.3. Immobilization of the metalloporphyrin

The preparation conditions of materials FeP-*s*GO (Fig. 1) are summarized in Table 5 and also consider the use of the conventional and microwave heating (entries 1–2), different reaction times (entries 1–3) and different solvents. The use of NMP as solvent was tested in order to improve the dispersibility of GO, as well as, to allow the reaction to be performed at higher temperature (entry 4). Finally, a direct reaction of FeP with non-silylated GO was performed (entry 5), in order to evaluate the relevance of the pre-functionalization with organosilane in the immobilization of the metalloporphyrin.

The most notorious change in the XRD diffractogram of material FeP-*sGOch1*, relatively to the precursors, is the significant decrease on the intensity of the (001) peak in accordance with the presence of new metalloporphyrin moieties in the interlayer space (Fig. 2). The (001) peak is observed at $2\theta = 12.6°$ (Table 2), corresponding to a d-spacing of 0.702 nm, and indicates an increase inter-planar spacing of 0.042 nm relatively to the precursor material *sGOch1* and of 0.138 nm relatively to original GO. The decrease of the (001) peak intensity and slight shifts of its position to lower 2θ in the XRD analysis were previously observed for immobilization of porphyrins on GO structures [25]. These evidences support the intercalation of the FeP on the interlayers of GO. It is worth to highlight that porphyrins are large planar structures with thickness of about 6–10 Å, which are structurally prone to intercalate between sheets of the obtained sGO materials.

The XPS atomic percentages indicated that after metalloporphyrin intercalation, the materials FeP-*sGOch1*, FeP-*sGOmw1* and FeP-*sGOmw2*, showed a decrease on C% and O% and that no bromine was detected on FeP-*s*GO materials (Table 3), while the presence of fluorine, nitrogen, iron and chlorine confirmed the presence of FeP.

The metalloporphyrin loading is similar in all materials, although a slightly higher immobilization was observed for nanohybrids obtained with microwave-assisted synthesis: the Fe% was 0.1% in conditions *ch1* (Table 5, entry1), corresponding to a concentration within the material of metalloporphyrin of 80 μmol·g^{-1} and 0.2% in conditions *mw1* and *mw2* (Table 5, entries 2 and 3), corresponding to a concentration of 150 μmol·g^{-1}. Concomitant variations in the atomic percentages of the other elements were observed. The absence of bromine and the presence of the FeP in the same loading than the observed for bromine in the silylated precursor material (150 μmol·g^{-1}), could indicate the reaction of bromoalkyl groups with the dimethylamino groups of the metalloporphyrin through covalent immobilization, although it can also indicate the reaction of the bromoalkyl moieties with

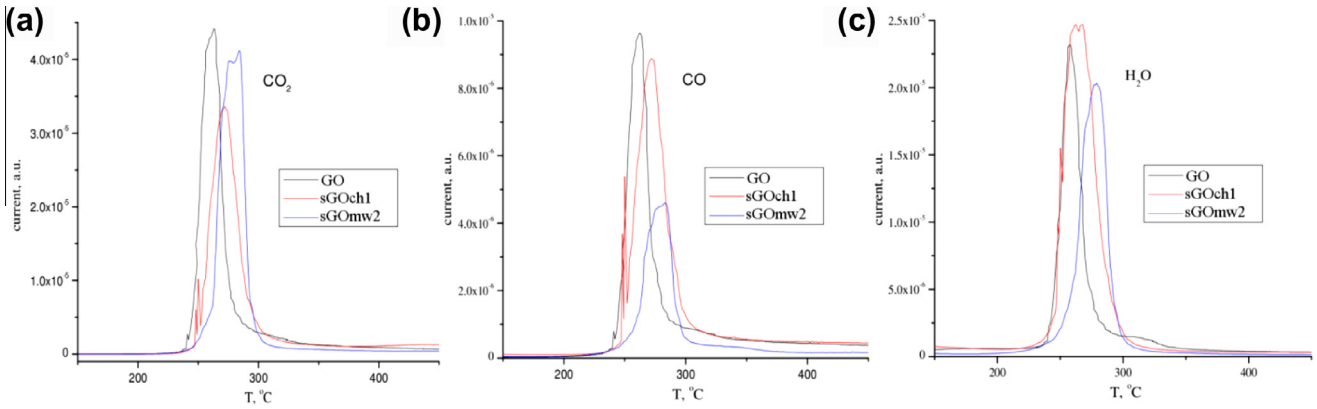

Fig. 6. Mass loss of the relevant molecular fragments in TPD analyzes for GO and silylated materials: (a) CO_2; (b) CO; (c) H_2O.

hydroxyl groups from GO, leading to the bromide release from the material.

As in the case of the silylation reaction, no advantage was observed in carrying out the metalloporphyrin immobilization reaction in microwave for longer reaction times than 1 h, since the XPS atomic percentages observed for conditions 2 and 3 were almost identical.

The high resolution XPS spectra of the relevant elements obtained for material FeP-*s*GO*mw1* are shown in Fig. 3c. In C1s and O1s regions no significant changes were observed relatively to the precursor material *s*GO*mw1*. In the N1s region of the FeP-*s*GO*mw1* spectrum only one band at 400.0 eV was observed and matches the contributions from the pyrrolic nitrogen in the porphyrin core and from the dimethylamine groups from the metalloporphyrin peripheral substituents [45]. The F1s spectrum shows an intense peak at 687.4 eV that is attributed to the fluorophenyl groups of the *meso*-position of the metalloporphyrin [46]. In the Fe2p3/2 region only one band with a maximum at 711.3 eV can be distinguished, due to the presence of Fe^{3+} thus providing confirmation for the presence of iron inside the porphyrin core [35]. In the Cl2p region of the spectrum, the band at 198.6 eV is attributed to chlorine coordinated to iron(III) in the core of the porphyrin and compares with the B.E. of chlorine in $FeCl_3$ at 198.8 eV [35]. The second peak can be ascribed to chloride ion. Similar deconvolution patterns and peak positions were observed for FeP-*s*GO*ch1* and FeP-*s*GO*mw2* materials (Fig. S3b and c; SI).

FTIR spectra of materials FeP-*s*GO (Fig. 4) show the characteristic bands of the organosilane, whereas in the spectra of materials FeP-sGO*mw2* and FeP-sGO*mw3* it can be distinguished small features at wavenumber below 1650 cm^{-1}, which can be assigned to intercalated metalloporphyrin. These bands are hardly observed in material FeP-sGO*ch* due to the lower FeP loading in the material. Furthermore, the spectrum of the material FeP-GO, resulting from the direct reaction of the FeP with pristine GO, matches the spectral pattern of original GO, revealing the inefficient functionalization.

The thermograms of FeP-*s*GO materials have similar mass loss pattern to those observed for the precursor materials (Fig. 5, Fig 2, SI). In Fig. 5, the thermogram of material FeP-sGO*ch1* is presented in comparison with the material sGO*ch1* and GO. The pronounced mass loss in the range of 200–300 °C occurs at exactly the same temperature as the precursor material *s*GO*ch1* ~240 °C, while in GO this mass loss occurs at ~250 °C. In the range of 280–800 °C, a progressive and lower rate of the mass loss occurs, which achieves a maximum of 42%. An equivalent value of 43% of the total mass loss was observed for the material prepared using microwave heating, namely FeP-*s*GO*mw2* (Table 5). In the studied temperature range the decomposition of the metalloporphyrin is not complete, achieving a maximum of 79%; however for hybrid materials, namely material FeP-*s*GO*mw2* increased mass loss relatively to the parent material is observed, as a confirmation of the porphyrin loading [39].

Catalytic oxidation tests were performed using *cis*-cyclooctene as a model substrate in order to obtain the proof of concept for the immobilization of the metalloporphyrin catalyst in its active form. The catalytic activity of the different hybrid materials was accessed using eco-sustainable conditions, namely, hydrogen peroxide as oxidant, in ethanol as reaction solvent and at room temperature [31].

The performance of the catalysts was shown to be proportional to the metalloporphyrin loading. When a rate of H_2O_2 addition of 0.5 $mmol{\cdot}h^{-1}$ was used (1 mol equivalents of oxidant relatively to the substrate per hour) the conversion after 2 h was 63% for material FeP-*s*GO*ch1*, showing a FeP loading of 80 $\mu mol{\cdot}g^{-1}$ (Table 6, entry 2) and 95% for material FeP-*s*GO*mw2*, showing a FeP loading of 150 $\mu mol{\cdot}g^{-1}$ (entry 8). The material FeP-*s*GO*mw3* did not show any catalytic activity after 2 h of reaction time (entry 12), suggesting that the immobilized iron(III) porphyrin is inactive, probably due to strong coordination of NMP (solvent used for its immobilization) onto the axial positions of the metal centre and thus avoiding the accessibility of H_2O_2 to the metal centre and consequently, imposing its inactivation. Furthermore, the material resulting from direct reaction of FeP with original GO (FeP-GO*mw*) did not show any catalytic behavior. This corroborates the absence of metalloporphyrin in this material as showed by FTIR. For all the previous assays the selectivity was 100% for the 1,2-epoxycyclooctane. A test control with GO material did not show any catalytic activity in epoxidation reaction, only a conversion $\leqslant$5% affording non identified products.

The test of material FeP-*s*GO*ch1* in the catalytic oxidation using a slower rate of H_2O_2 addition of 0.25 $mmol{\cdot}h^{-1}$ (entries 4–6) led to higher substrate conversations relatively to the observed with the rate of 0.5 $mmol{\cdot}h^{-1}$ (entries 1–3). The results can be rationalized by the lower stability of the catalyst in the higher oxidizing medium. The progress of conversion with time demonstrated that a rate of H_2O_2 addition at 0.25 $mmol{\cdot}h^{-1}$ established the kinetic control of the reaction. The results evidence a molecular reactivity of hydrogen peroxide-substrate in a stoichiometry close to 1:1 and show the high efficiency of H_2O_2 activation with these catalytic systems, even at low oxidant concentrations.

In the overall, the results support the relevance of the silylation reaction for further metalloporphyrin immobilization, confirming that the increase in the interlayer distance obtained upon silylation allowed the final metalloporphyrin entrapment. This may have occurred by physical entrapment of the FeP molecules between GO layers or by covalent bonding; this latter reaction was tested with success on MWCNT decorated with hydroxyl groups [35],

Table 6
Catalytic epoxidation of *cis*-cyclooctene by H_2O_2 in ethanol.[a]

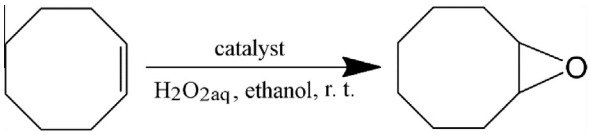

Entry	Reaction	Catalyst	H_2O_2 (mmol·h^{-1})[b]	*t* (h)	C%[c]	TON	TOF (h^{-1})[d]
1	1	FeP-*s*GO*ch1*	0.5	1	60	150	77
2				2	63	158	
3				3	64	160	
4	2		0.25	1	47	118	60
5				2	77	192	
6				3	78	195	
7	3	FeP-*s*GO*mw2*	0.5	1	90	118	115
8				2	93	122	
9				5	95	125	
10	4	FeP-*s*GO*mw3*	0.5	2	0	0	0
11	5	FeP-GO*mw*	0.5	2	0	0	0
12	6	FeP	0.5	1	100	141	128

[a] Reaction conditions: the substrate (0.5 mmol) and catalyst (25 mg of FeP-*s*GO or 4 mg of FeP, corresponding to the same mass loaded in 25 mg of material) were stirred in 1.5 mL of ethanol at room temperature and H_2O_2 was progressively added to the reaction.
[b] Rate of addition of H_2O_2 to the reaction mixture.
[c] Substrate conversion was determined by GC analyses, as well as, the selectivity that in all cases was 100% since 1,2-epoxycyclooctane was the only product.
[d] Calculated after the first hour of the reaction.

where efficient entrapment is not prone to occur. The π–π staking of FeP on GO is less probable due to the small (2–3 nm) aromatic domains and the hampering arising from the functional groups that are expected to be present on GO, as well as, the high planar dimensions of the metalloporphyrin macromolecule; ionic interactions are not expected as well.

4. Conclusions

GO was silylated by an alkylbromosilane and this material was used as a host material for the intercalation of a Fe(III) porphyrin. The reaction performed under microwave heating in toluene during 1 h led to the best metalloporphyrin loading. Longer reaction times did not led to further improvements on the metalloporphyrin loading. A significant reduction of the reaction time, energy consumption and better maintenance of material integrity was obtained relatively to conventional heating. The results indicate some silane polymerization despite the use of anhydrous and apolar solvent and reaction on both methoxy silyl and alkylbromide moieties. Materials silylation facilitates the maintenance of a stacked structure with a higher interlayer distance and allowed the intercalation of the ironporphyrin on its catalytic-active form.

Acknowledgments

The authors thank the Fundação para a Ciência e a Tecnologia (FCT, Portugal), the European Union, QREN, FEDER, COMPETE, for funding REQUIMTE through projects PEst-C/EQB/LA0006/2013, NORTE-07-0124-FEDER-000067-nanochemistry and PTDC/EQU-ERQ/110825/2009. Authors acknowledge the MICINN of Spain (Projects CTQ-2011-29272-C04-01 and -03) for financial support. Thanks are also due to Joint Project "Acções Luso-Espanholas" E20/11 Acciones Integradas AIB2010PT-00104. Monika E. Lipińka also thanks FCT for a PhD grant SFRH/BD/66297/2009.

Appendix A. Supplementary data

Supplementary data associated with this article can be found, in the online version, at http://dx.doi.org/10.1016/j.poly.2014.07.003.

References

[1] D.R. Dreyer, S. Park, C.W. Bielawski, R.S. Ruoff, Chem. Soc. Rev. 39 (2010) 228.
[2] M. Jahan, Q. Bao, K.P. Loh, J. Am. Chem. Soc. 134 (2012) 6707.
[3] M.L. Yola, N. Atar, Z. Üstündag, A.O. Solak, J. Electroanal. Chem. 698 (2013) 9.
[4] Y. Zhu, S. Murali, W. Cai, X. Li, J.W. Suk, J.R. Potts, R.S. Ruoff, Adv. Mater. 22 (2010) 3906.
[5] M.J. Allen, V.C. Tung, R.B. Kaner, Chem. Rev. 110 (2010) 132.
[6] Y. Dong, J. Li, L. Shi, J. Xu, X. Wang, Z. Guo, W. Liu, J. Mater. Chem. A 1 (2013) 644.
[7] Y. Yang, Y.M. Zhang, Y. Chen, D. Zhao, J.T. Chen, Y. Liu, Chem. Eur. J. 18 (2012) 4208.
[8] C. Su, K.P. Loh, Acc. Chem. Res. 46 (2013) 2275.
[9] W. Zhang, S. Wang, J. Ji, Y. Li, G. Zhang, F. Zhang, X. Fan, Nanoscale 5 (2013) 6030.
[10] Z. Li, S. Wu, H. Ding, D. Zheng, J. Hu, X. Wang, Q. Huo, J. Guan, Q. Kan, New J. Chem. 37 (2013) 1561.
[11] A.B. Dongil, B. Bachiller-Baeza, A. Guerrero-Ruiz, I. Rodríguez-Ramos, J. Cat. 282 (2011) 299.
[12] S. Stankovich, D.A. Dikin, R.D. Piner, K.A. Kohlhaas, A. Kleinhammes, Y. Jia, Y. Wu, Carbon 45 (2007) 1558.
[13] J.W. Burress, S. Gadipelli, J. Ford, J.M. Simmons, W. Zhou, T. Yildirim, Angew. Chem., Int. Ed. 49 (2010) 8902.
[14] Y. Matsuo, Y. Tachibana, K. Konishi, Carbon 50 (2012) 5346.
[15] A. Shanmugharaj, J.H. Yoon, W.J. Yang, S.H. Ryu, J. Colloid Interface Sci. 401 (2013) 148.
[16] W.S. Ma, J. Li, X.S. Zhao, J. Mater. Sci. 48 (2013) 5287.
[17] X. Wang, W. Xing, P. Zhang, L. Song, H. Yang, Y. Hu, Compos. Sci. Technol. 72 (2012) 737.
[18] Y. Matsuo, T. Fukunaga, T. Fukutsuka, Y. Sugie, Carbon 42 (2004) 2113.
[19] H. Gaspar, C. Pereira, S.L.H. Rebelo, M.F.R. Pereira, J.L. Figueiredo, C. Freire, Carbon 49 (2011) 3441.
[20] A.B. Dongil, B. Bachiller-Baeza, A. Guerrero-Ruiz, I. Rodríguez-Ramos, Catal. Commun 26 (2012) 149.
[21] Y. Matsuo, K. Iwasa, Y. Sugie, A. Mineshige, H. Usami, Carbon 48 (2010) 4009.
[22] Y. Matsuo, Y. Nishino, T. Fukutsuka, Y. Sugie, Carbon 45 (2007) 1384.
[23] A.B. Bourlinos, D. Gournis, D. Petridis, T. Szabo, A. Szeri, I. Dekany, Langmuir 19 (2003) 6050.
[24] M.E. Lipińska, D.M.D. Teixeira, C.A.T. Laia, A.M.G. Silva, S.L.H. Rebelo, C. Freire, Tetrahedron Lett. 54 (2013) 110.
[25] A. Wang, L. Long, W. Zhao, Y. Song, M.G. Humphrey, M.P. Cifuentes, Xingzhi Wu, Y. Fu, D. Zhang, X. Li, C. Zhang, Carbon 53 (2013) 327.
[26] M.B.M. Krishna, N. Venkatramaiah, R. Venkatesan, D.N. Rao, J. Mater. Chem. 22 (2012) 3059.
[27] A. Hassanpour, D. Rodriguez-San Miguel, J.L.G. Fierro, B.R. Horrocks, R. Mas-Ballesté, F. Zamora, Chem. Eur. J. 19 (2013) 10463.
[28] Q. Wang, J. Lei, Sh. Deng, L. Zhang, H. Ju, Chem. Commun. 49 (2013) 916.
[29] R. Weinstain, E.N. Savariar, C.N. Felsen, R.Y. Tsien, J. Am. Chem. Soc. 136 (2014) 874.
[30] T. Xue, S. Jiang, Y. Qu, Q. Su, R. Cheng, S. Dubin, C.Y. Chiu, R. Kaner, Y. Huang, X. Duan, Angew. Chem., Int. Ed. 51 (2012) 3822.

[31] S.L.H. Rebelo, M. Linhares, M.M.Q. Simões, A.M.S. Silva, M.G.P.M.S. Neves, J.A.S. Cavaleiro, C. Freire, J. Catal. 315 (2014) 33.
[32] P. Costa, M. Linhares, S.L.H. Rebelo, M.G.P.M.S. Neves, C. Freire, RSC Adv. 3 (2013) 5350.
[33] S.L.H. Rebelo, M.M. Pereira, P.V. Monsanto, H.D. Burrows, J. Mol. Catal. A: Chem. 297 (2009) 35.
[34] M.E. Lipińska, S.L.H. Rebelo, C. Freire, J. Mater. Sci. 49 (2014) 1494.
[35] M. Melucci, E. Treossi, L. Ortolani, G. Giambastiani, V. Morandi, P. Klar, C. Casiraghi, P. Samorìae, V. Palermo, J. Mater. Chem. 20 (2010) 9052.
[36] B. Brodie, Philos. Trans. R. Soc. Lond. 149 (1859) 249.
[37] R.A.W. Johnstone, M.L.P.G. Nunes, M.M. Pereira, A.M.A.R. Gonsalves, A.C. Serra, Heterocycles 43 (1996) 1423.
[38] M. Linhares, S.L.H. Rebelo, M.M.Q. Simoes, A.M.S. Silva, M.G.P.M.S. Neves, J.A.S. Cavaleiro, C. Freire, Appl. Catal. A: Gen. 470 (2014) 427.
[39] M.E. Lipińska, S.L.H. Rebelo, M.F.R. Pereira, J.L. Figueiredo, C. Freire, Mater. Chem. Phys. 143 (2013) 296.
[40] Y. Matsuo, T. Tabata, T. Fukunaga, T. Fukutsuka, Y. Sugie, Carbon 43 (2005) 2875.
[41] A. Lerf, H. Heyong, M. Forster, J. Klinowski, J. Phys. Chem. B 102 (1998) 4477.
[42] G. Socrates, Infrared and Raman characteristic group frequencies. Tables and charts, 3th ed, Jonh Wiley & Sons Ltd, Chichester, 1995.
[43] I. Jung, D.A. Field, N.J. Clark, Y. Zhu, D. Yang, R.D. Piner, S. Stankovich, D.A. Dikin, H. Geisler, C.A. Ventrice Jr., R.S. Ruof, J. Phys. Chem. C 113 (2009) 18480.
[44] P. Solís-Fernández, R. Rozada, J.I. Paredes, S. Villar-Rodil, M.J. Fernández-Merino, L. Guardia, A. Martínez-Alonso, J.M.D. Tascón, J. Alloy Compd. 536 (2012) S532.
[45] C.D. Wagner, J.F. Moulder, L.E. Davis, W.M. Riggs, Handbook of X-ray photoelectron spectroscopy, Perkin-Elmer Corporation, Physical Electronics Division, Eden Prairie, Minnesota, 1973.
[46] M.E. Lipińska, S.L.H. Rebelo, M.F.R. Pereira, J.A.N.F. Gomes, C. Freire, J.L. Figueiredo, Carbon 50 (2012) 3280.